

Femtoscopic signatures of unique nuclear structures in relativistic collisions

Dániel Kincses*

ELTE Eötvös Loránd University, Pázmány Péter sétány 1/A, H-1117 Budapest, Hungary

(Dated: June 9, 2025)

One of the most vital topics of today's high-energy nuclear physics is the investigation of the nuclear structure of the collided nuclei. Recent studies at the Relativistic Heavy Ion Collider (RHIC) and the Large Hadron Collider (LHC) have shown that several observables, such as the collective flow and transverse-momentum correlations of the produced particles, can be sensitive to various nuclear structure and deformation parameters. Femtoscopy, another essential tool for investigating the space-time geometry of the matter created in nuclear collisions, has not yet been widely applied to such studies. Using a multiphase transport model (AMPT), in this Letter, it is demonstrated that the femtoscopic source parameters of pion pairs can also serve as a robust signal of unique nuclear structure. Through an analysis of $^{208}\text{Pb}+^{20}\text{Ne}$ and $^{208}\text{Pb}+^{16}\text{O}$ collisions at $\sqrt{s_{NN}} = 68.5$ GeV, two collision systems especially relevant to the SMOG2 program of the LHCb experiment, it is shown that a deformed initial shape can significantly affect femtoscopic source parameters. This study highlights the importance of expanding the nuclear structure investigations to femtoscopic observables and serves as a baseline for numerous possible future studies in this new direction.

I. INTRODUCTION

In recent years, the high-energy nuclear physics community has shown significant interest in the possibility of imaging nuclear structures in high-energy collisions [1–8]. One of the main tools in the arsenal of measurements is the anisotropic flow of particles created in nuclear collisions [9]. In fluid-dynamical descriptions of nuclear collisions, it has been shown that the momentum anisotropy of the particles originates from the azimuthal anisotropy of the initial density profile of the fireball [10]. Measuring the Fourier coefficients v_n of the single particle azimuthal distributions and investigating their correlations with transverse momentum have become widely used tools for characterizing the parameters of initial-state nuclear deformation [11–17].

Another important subfield of high-energy physics, femtoscopic correlation measurements [18], has not yet been widely utilized to study the nuclear structure. Such measurements provide a highly versatile tool for investigating the space-time geometry of the particle-emitting source created in high-energy nuclear collisions [19, 20]. At the core of femtoscopy is the so-called Koonin-Pratt equation [21–23]:

$$C_2(\vec{q}, \vec{K}) = \int d^3\vec{\rho} D_{\vec{K}}(\vec{\rho}) |\psi_{\vec{q}}(\vec{\rho})|^2, \quad (1)$$

which connects the C_2 two-particle momentum correlation function to the D spatial correlation function, also known as the pair source function. The momentum correlation function depends on the pair relative momentum \vec{q} and the average pair momentum \vec{K} , while the pair source function depends on the relative pair separation $\vec{\rho}$. In case of bosonic particles (e.g., pions), the

$\Psi_{\vec{q}}(\vec{\rho})$ quantum-mechanical pair wave function is symmetrized, thus in the interaction-free case the momentum correlation will be equal to the Fourier-transform of the pair source function [24]. In experimental analyses, the pair source is often indirectly studied through C_2 [25, 26], or reconstructed via an imaging method [27–30]. In event generator models, such as the multi-phase transport model (AMPT), the full phase-space information is available for the created particles, including the freeze-out coordinates. Therefore, the pair source can be directly reconstructed and studied.

Recent experimental measurements [31–35] and phenomenological studies [24, 36–39] showed that the shape of the pion pair-source in high-energy collisions can be described by an elliptically contoured symmetric Lévy-stable distribution:

$$D(\vec{\rho}) = \mathcal{L}(\alpha, R^2, \vec{\rho}) = \int \frac{d^3\vec{q}}{(2\pi)^3} e^{i\vec{q}\cdot\vec{\rho}} e^{-\frac{1}{2}|\vec{q}^T R^2 \vec{q}|^{\alpha/2}}, \quad (2)$$

where α is called the Lévy-exponent, characterizing the power-law tail of the source, and R^2 is a symmetric 3×3 matrix, containing the 6 independent Lévy-scale parameters. These, in the case of Gaussian parameterization of the source function (corresponding to the special $\alpha = 2$ case), are often referred to as the HBT-radii parameters after Hanbury Brown and Twiss, who invented the intensity-interferometry technique in radio astronomy [40, 41].

For the sake of simplicity, the experimental measurements are often angle-averaged [31–35], extracting only a single scale parameter. Three-dimensional investigations [36, 42] are more complicated, but can reveal further details about the freeze-out source. A common observation of the extracted scale parameters (be it angle-averaged or multi-dimensional) is that they systematically decrease with the average transverse momentum of the pair. This property is often attributed to collective flow [43–46]. Thus, measurements that are integrated over the azimuthal angle of the pair relative to the re-

* kincses@ttk.elte.hu

action plane cannot probe the entire volume of the fireball created in the collision [43]. However, in the case of analyses performed relative to the reaction plane [44–50], azimuthal oscillations of the scale parameters have been shown to be connected to the shape of the entire fireball [51]. This property will be the focus of the current manuscript, with emphasis on the connection of HBT radii oscillations to the initial nuclear structure of the collided nuclei.

II. METHODS

To assess the sensitivity of azimuthal femtoscopic measurements to nuclear structure, $^{208}\text{Pb}+^{20}\text{Ne}$ and $^{208}\text{Pb}+^{16}\text{O}$ collisions at $\sqrt{s_{NN}} = 68.5$ GeV are studied, two systems especially relevant to the SMOG2 fixed-target program of the LHCb experiment [52–54]. Using the AMPT parton transport model [55], two different initial nucleon configurations are investigated in each case: the spherically symmetric Woods-Saxon configuration [56] and the Nuclear Lattice Effective Field Theory (NLEFT) configuration where nucleons are distributed in a manner that resembles α -clusters [57]. The latter results in a tetrahedron shape for the oxygen nucleus resembling four α -clusters, and a bowling pin shape resembling five α -clusters for the neon nucleus. The initial nucleon configurations were also rotated randomly. With similar model configurations, it has already been shown [58, 59] that the azimuthal anisotropy is sensitive to the deformed initial shape of the neon nucleus. However, femtoscopic observables have not yet been investigated.

For this study, 100,000 ultra-central ($b = 0$) events were simulated for each collision system (Pb+Ne and Pb+O) and for each nucleon configuration (Woods-Saxon and NLEFT). The pseudo-rapidity acceptance of the LHCb experiment is around $2 < \eta < 5$ in the laboratory frame, which roughly corresponds to $-2.5 < \eta < 0.5$ in the center-of-mass frame in the case of fixed-target collisions [54]; thus, only particles within this η range were used for the present analysis. To determine the second-order event plane, charged pions, kaons, and protons in the rapidity range of $-2.5 < \eta < -0.5$ were used. For the femtoscopic analysis, charged pions were chosen in the kinematic range of $-0.5 < \eta < 0.5$ and $0.2 < p_T [\text{GeV}/c] < 1.0$. The second-order event plane angle Ψ_2 was calculated similarly to Ref. [47], with the Q_x and Q_y flow-vectors defined as

$$\Psi_2 = \frac{1}{2} \arctan \left(\frac{Q_y}{Q_x} \right), \quad (3)$$

$$Q_x = \frac{1}{N} \sum_i w_i \cos(2\phi_i), \quad (4)$$

$$Q_y = \frac{1}{N} \sum_i w_i \sin(2\phi_i), \quad (5)$$

where N is the total number of particles, the w_i weight is equal to the p_T transverse momentum of the particle, and ϕ is the azimuthal angle of the particle.

To construct the pion pair source distribution, same-charge pion pairs were chosen in 5 different ranges of average transverse momentum k_T , and 15 different ranges of pair azimuthal angle relative to the second-order event plane. The components of the $D(\vec{\rho})$ source distribution were calculated in the Bertsch-Pratt coordinate frame, where the 'out' direction is along the average transverse momentum of the pair, 'long' is the beam direction, and 'side' is perpendicular to the other two. A boost to the Longitudinal Co-Moving System (LCMS) was also applied (see Equations 13-15 of Ref. [36]). Following the methodology of Ref. [36], one-dimensional projections of the three-dimensional source distribution were constructed along six different directions corresponding to the following unit vectors:

$$\begin{aligned} \vec{e}^{(o)} &= (1, 0, 0), & \vec{e}^{(os)} &= \frac{1}{\sqrt{2}}(1, 1, 0), \\ \vec{e}^{(s)} &= (0, 1, 0), & \vec{e}^{(ol)} &= \frac{1}{\sqrt{2}}(1, 0, 1), \\ \vec{e}^{(l)} &= (0, 0, 1), & \vec{e}^{(sl)} &= \frac{1}{\sqrt{2}}(0, 1, 1). \end{aligned} \quad (6)$$

Similarly to Ref. [36], in the case of a given k_T and $\varphi_{\text{pair}} - \Psi_2$ range, one-dimensional Lévy-stable distributions were fitted simultaneously to the six projections, with seven free parameters: the six independent Lévy-scale parameters of the R^2 matrix, and the same Lévy-exponent parameter α . The one-dimensional Lévy-stable distributions are defined as [60]

$$\mathcal{L}^{1D}(\rho_\nu, \alpha, R_\nu) = \frac{1}{2\pi} \int dq e^{iq\rho_\nu} e^{-\frac{1}{2}|qR_\nu|^\alpha}, \text{ where} \\ \rho_\nu = \vec{e}^{(\nu)} \cdot \vec{\rho}, \quad R_\nu = \sqrt{\vec{e}^{(\nu),T} R^2 \vec{e}^{(\nu)}}, \quad \text{and} \\ \nu = o, s, l, os, ol, sl. \quad (7)$$

An example fit is shown in Figure 1.

After extracting the source parameters, their $\varphi_{\text{pair}} - \Psi_2$ dependence were investigated in each k_T bin. For the azimuthal dependence of the scale parameters the following parametrization were used [47]:

$$R_\mu^2(\varphi_{\text{pair}} - \Psi_2) = R_{\mu,0}^2 + 2R_{\mu,2}^2 \cos(2(\varphi_{\text{pair}} - \Psi_2)), \\ \text{if } \mu = \text{out, side, long, out-long} \quad (8)$$

and

$$R_\mu^2(\varphi_{\text{pair}} - \Psi_2) = R_{\mu,0}^2 + 2R_{\mu,2}^2 \sin(2(\varphi_{\text{pair}} - \Psi_2)), \\ \text{if } \mu = \text{out-side, side-long}. \quad (9)$$

An example set of parameters in a given k_T bin, with fits corresponding to Equations 8-9, is shown in Figure 2.

III. RESULTS AND DISCUSSION

As illustrated by Figure 1, the three-dimensional elliptically contoured Lévy-stable distribution provides a

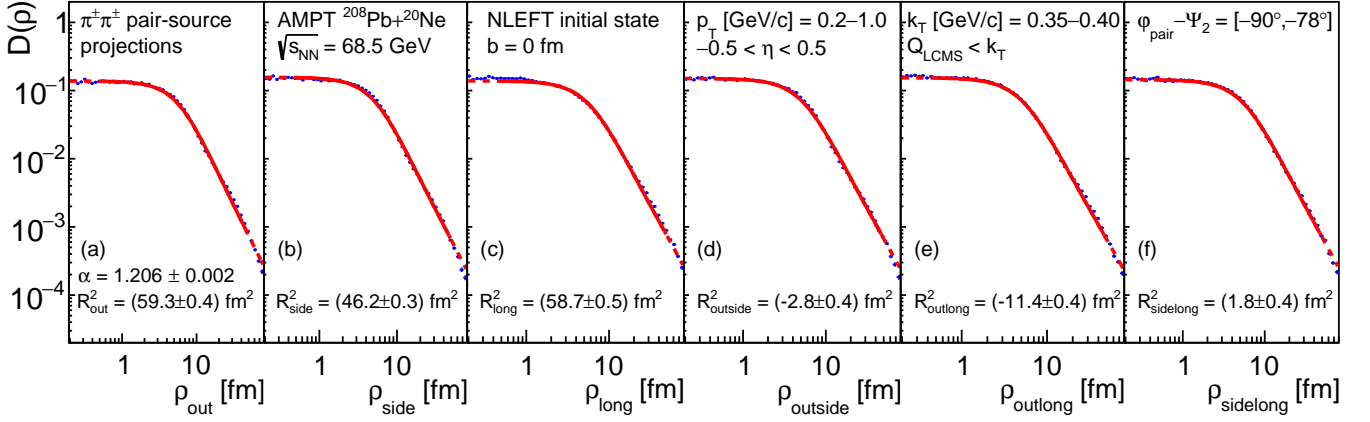


FIG. 1. An example simultaneous fit to six projections of the three-dimensional source distribution of the same charge pion pairs, reconstructed in AMPT simulations of $\sqrt{s_{NN}} = 68.5$ GeV Pb+Ne collisions with the NLEFT initial state nucleon configuration. Panels (a)-(f) show the one-dimensional projections of $D(\vec{\rho})$ with blue markers, corresponding to the directions detailed in Equation 6. The fit with one-dimensional Lévy-stable distributions, as described by Equation 7, is shown with red lines.

good description of the source shape, capturing the apparent power-law tail of the pion pair source (which would not be possible with the Gaussian approximation often applied in similar studies [61]). This is the first investigation where all six independent scale parameters of the Lévy-stable pion pair source are determined, as all previous analyses were azimuthally integrated [24, 31–39].

Figure 2 shows the azimuthal angle dependence of the extracted source parameters in Pb+Ne collisions. As expected, the Lévy scale parameter α shown in panel (a) does not depend strongly on the azimuthal angle, and a constant fit provides a good description. There is a small systematic difference between the Woods-Saxon and NLEFT configurations, but it is most probably below the achievable experimental precision. The extracted Lévy-scale parameters are shown in the other panels, fitted with the parametrization described in Equations 8-9. Panels (b)-(d) show the diagonal elements of the radii matrix, where a clear separation between the Woods-Saxon and the NLEFT configurations can be observed in the out and side directions. Panels (e)-(f) show the off-diagonal elements, where interestingly, each direction exhibits a zeroth-order Fourier term, probably due to the collision-system asymmetry. Some of these parameters already show differences between the two initial nucleon configurations, however, a more robust signal can be expected in the case of relative oscillations.

It has been shown that the relative oscillation (i.e., the ratio of the second to the zeroth order Fourier terms) of the R_{side}^2 parameter is connected to the freeze-out eccentricity of the fireball around the beam direction [47]:

$$\varepsilon_F = 2 \frac{R_{\text{side},2}^2}{R_{\text{side},0}^2}. \quad (10)$$

The dependence of the extracted freeze-out eccentric-

ity on the average transverse mass $m_T = \sqrt{k_T^2 + m_\pi^2}$ is shown in Figure 3, for both Pb+Ne and Pb+O collisions. For each of the four cases, a slight increase towards higher m_T can be observed. The oxygen results do not exhibit any significant differences between the NLEFT and Woods-Saxon cases, as the clustering-like structure in this case does not increase the elliptical asymmetry. On the other hand, the elliptical asymmetry caused by the bowling-pin shape of the neon nucleus seems to persist through the hadronic phase and significantly increase the freeze-out eccentricity compared to the spherical Woods-Saxon configuration, as well as compared to any of the oxygen configurations. It is also interesting to note that between the two Woods-Saxon cases, the neon eccentricity seems to be systematically below the oxygen, probably due to the slightly larger size of the system. Thus, the freeze-out eccentricity determined from azimuthally sensitive pion femtoscopy could provide another robust signal for the deformed initial shape of the neon nucleus when compared with oxygen measurements.

IV. SUMMARY AND OUTLOOK

This study presents an analysis of $\sqrt{s_{NN}} = 68.5$ GeV $^{208}\text{Pb} + ^{20}\text{Ne}$ and $^{208}\text{Pb} + ^{16}\text{O}$ collisions, simulated with the AMPT hadronic transport model. For each collision system two different initial nucleon configurations are investigated: the spherical Woods-Saxon model, and the NLEFT model where the nucleons are distributed in a manner that resembles α -clusters. The pion pair source distribution is investigated in various average transverse mass m_T ranges and pair azimuthal angle ranges relative to the second order event plane. It is shown that a three-dimensional Lévy-stable distribution provides a good approximation for the source shape and the Lévy-exponent α and R^2 Lévy-scale matrix parameters are determined.

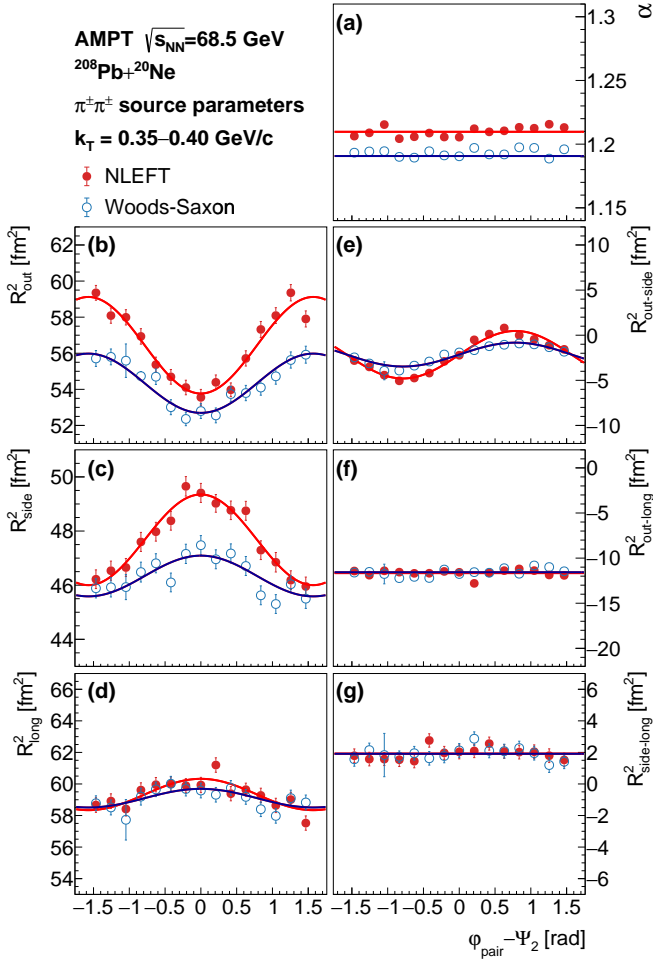


FIG. 2. Extracted pion pair source parameters in $\sqrt{s_{NN}} = 68.5$ GeV $^{208}\text{Pb} + ^{20}\text{Ne}$ collisions generated by AMPT, as a function of pair azimuthal angle relative to the second order event plane, in the average transverse momentum range of $0.35 < k_T$ (GeV/c) < 0.40 . The source parameter values and their statistical uncertainties are shown with filled red markers and error bars for the NLEFT configuration, and empty blue markers and error bars for the Woods-Saxon configuration. Panel (a) shows the Lévy-exponent parameter α , while panels (b)-(g) show the elements of the R^2 Lévy-scale parameter matrix. For each dataset, a fit is shown as well corresponding to Equations 8 and 9.

Subsequently, from the azimuthal oscillation of the R^2_{side} scale parameter the zeroth and second order Fourier components are determined, and from their ratio the freeze-out eccentricity is calculated. This observable is found

to be significantly increased in the NLEFT configuration of Pb+Ne collisions compared to the other three cases. When comparing the Woods-Saxon configurations, it is found that the Pb+Ne eccentricity is systematically below the Pb+O result. Thus, the freeze-out eccentricity determined simultaneously in Pb+Ne and Pb+O collisions from azimuthal sensitive pion femtoscopy could provide another robust signal for the deformed initial shape of the neon nucleus.

Femtoscopy is a rich field with many more directions to explore regarding possible future nuclear structure studies. The azimuthal sensitive analysis could be extended to non-identical particle femtoscopy, as well as to higher order event planes where similar relative oscillations of the scale parameters might provide more insight.

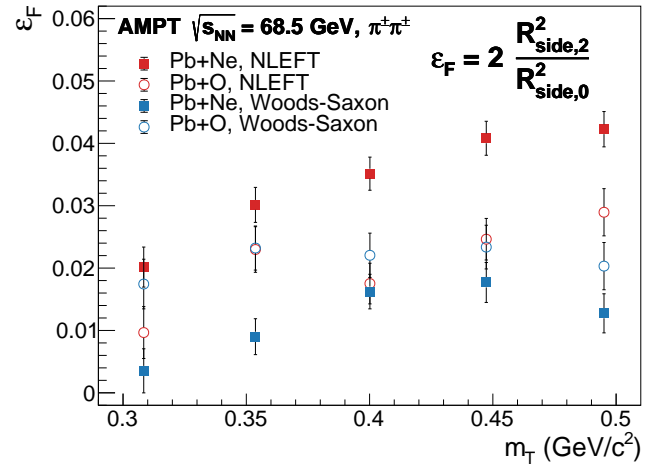


FIG. 3. Average transverse mass dependence of the freeze-out eccentricity calculated for four different configurations. The NLEFT and Woods-Saxon initial state configurations are plotted with red and blue markers, respectively. The Pb+Ne result is plotted with filled markers, while the Pb+O result is plotted with empty markers.

ACKNOWLEDGMENTS

The author is grateful to You Zhou, Máté Csanád, and Márton Nagy for their feedback and discussions. This research was funded by the NKFIH grants TKP2021-NKTA-64, PD-146589, and K-138136. D. K. was supported by the EKÖP-24 University Excellence Scholarship program of the Ministry for Culture and Innovation from the source of the national research, development, and innovation fund.

[1] G. Giacalone, J. Jia, and C. Zhang, Impact of Nuclear Deformation on Relativistic Heavy-Ion Collisions: Assessing Consistency in Nuclear Physics across En-

ergy Scales, Phys. Rev. Lett. **127**, 242301 (2021), arXiv:2105.01638 [nucl-th].

[2] B. Bally, M. Bender, G. Giacalone, and V. Somà, Ev-

- idence of the triaxial structure of ^{129}Xe at the Large Hadron Collider, Phys. Rev. Lett. **128**, 082301 (2022), arXiv:2108.09578 [nucl-th].
- [3] G. Giacalone, G. Nijs, and W. van der Schee, Determination of the Neutron Skin of Pb208 from Ultrarelativistic Nuclear Collisions, Phys. Rev. Lett. **131**, 202302 (2023), arXiv:2305.00015 [nucl-th].
- [4] C. Zhang and J. Jia, Evidence of Quadrupole and Octupole Deformations in Zr96+Zr96 and Ru96+Ru96 Collisions at Ultrarelativistic Energies, Phys. Rev. Lett. **128**, 022301 (2022), arXiv:2109.01631 [nucl-th].
- [5] S. Zhao, H.-j. Xu, Y. Zhou, Y.-X. Liu, and H. Song, Exploring the Nuclear Shape Phase Transition in Ultra-Relativistic $^{129}\text{Xe}+^{129}\text{Xe}$ Collisions at the LHC, Phys. Rev. Lett. **133**, 192301 (2024), arXiv:2403.07441 [nucl-th].
- [6] R. A. Lacey, Anisotropy scaling functions in heavy-ion collisions: Insights into the ultracentral flow puzzle and constraints on transport coefficients and nuclear deformation, Phys. Rev. C **110**, L031901 (2024), arXiv:2402.09389 [nucl-ex].
- [7] S. Prasad, N. Mallick, R. Sahoo, and G. G. Barnaföldi, Anisotropic flow fluctuation as a possible signature of clustered nuclear geometry in O-O collisions at the Large Hadron Collider, Phys. Lett. B **860**, 139145 (2025), arXiv:2407.15065 [nucl-th].
- [8] N. Magdy, M. Hegazy, A. Rafaat, W. Li, A. Deshpande, A. M. H. Abdelhady, A. Y. Ellithi, R. A. Lacey, and Z. Tu, A study of nuclear structure of light nuclei at the electron-ion collider, Eur. Phys. J. A **60**, 212 (2024), arXiv:2405.07844 [nucl-th].
- [9] J.-Y. Ollitrault, Anisotropy as a signature of transverse collective flow, Phys. Rev. D **46**, 229 (1992).
- [10] H. Niemi, G. S. Denicol, H. Holopainen, and P. Huovinen, Event-by-event distributions of azimuthal asymmetries in ultrarelativistic heavy-ion collisions, Phys. Rev. C **87**, 054901 (2013), arXiv:1212.1008 [nucl-th].
- [11] G. Giacalone, F. G. Gardim, J. Noronha-Hostler, and J.-Y. Ollitrault, Correlation between mean transverse momentum and anisotropic flow in heavy-ion collisions, Phys. Rev. C **103**, 024909 (2021), arXiv:2004.01765 [nucl-th].
- [12] S. Acharya *et al.* (ALICE), Anisotropic flow in Xe-Xe collisions at $\sqrt{s_{\text{NN}}} = 5.44$ TeV, Phys. Lett. B **784**, 82 (2018), arXiv:1805.01832 [nucl-ex].
- [13] S. Acharya *et al.* (ALICE), Pseudorapidity dependence of anisotropic flow and its decorrelations using long-range multiparticle correlations in Pb-Pb and Xe-Xe collisions, Phys. Lett. B **850**, 138477 (2024), [Erratum: Phys. Lett. B **853**, 138659 (2024)], arXiv:2307.11116 [nucl-ex].
- [14] M. I. Abdulhamid *et al.* (STAR), Imaging shapes of atomic nuclei in high-energy nuclear collisions, Nature **635**, 67 (2024), arXiv:2401.06625 [nucl-ex].
- [15] G. Aad *et al.* (ATLAS), Correlations between flow and transverse momentum in Xe+Xe and Pb+Pb collisions at the LHC with the ATLAS detector: A probe of the heavy-ion initial state and nuclear deformation, Phys. Rev. C **107**, 054910 (2023), arXiv:2205.00039 [nucl-ex].
- [16] E. G. D. Nielsen, N. Nathanson, K. Gulbrandsen, and Y. Zhou, A unified algorithm for multi-particle correlations between azimuthal angle and transverse momentum in ultra-relativistic nuclear collisions (2025), arXiv:2504.03044 [nucl-th].
- [17] E. G. D. Nielsen, F. K. Rømer, K. Gulbrandsen, and Y. Zhou, Generic multi-particle transverse momentum correlations as a new tool for studying nuclear structure at the energy frontier, Eur. Phys. J. A **60**, 38 (2024), arXiv:2312.00492 [nucl-th].
- [18] M. A. Lisa, S. Pratt, R. Soltz, and U. Wiedemann, Femtoscopy in relativistic heavy ion collisions, Ann. Rev. Nucl. Part. Sci. **55**, 357 (2005), arXiv:nucl-ex/0505014.
- [19] Csörgő, T., Particle interferometry from 40-MeV to 40-TeV, Acta Phys. Hung. A **15**, 1 (2002), arXiv:hep-ph/0001233.
- [20] U. A. Wiedemann and U. W. Heinz, Particle interferometry for relativistic heavy ion collisions, Phys. Rept. **319**, 145 (1999), arXiv:nucl-th/9901094.
- [21] F. B. Yano and S. E. Koonin, Determining Pion Source Parameters in Relativistic Heavy Ion Collisions, Phys. Lett. B **78**, 556 (1978).
- [22] S. Pratt, Pion Interferometry for Exploding Sources, Phys. Rev. Lett. **53**, 1219 (1984).
- [23] S. Pratt, Validity of the smoothness assumption for calculating two-boson correlations in high-energy collisions, Phys. Rev. C **56**, 1095 (1997).
- [24] M. Nagy, A. Purzsa, M. Csanád, and D. Kincses, A novel method for calculating Bose-Einstein correlation functions with Coulomb final-state interaction, Eur. Phys. J. C **83**, 1015 (2023), arXiv:2308.10745 [nucl-th].
- [25] S. S. Adler *et al.* (PHENIX), Bose-Einstein correlations of charged pion pairs in Au + Au collisions at $s(\text{NN})^{1/2} = 200$ -GeV, Phys. Rev. Lett. **93**, 152302 (2004), arXiv:nucl-ex/0401003.
- [26] J. Adams *et al.* (STAR), Pion interferometry in Au+Au collisions at $S(\text{NN})^{1/2} = 200$ -GeV, Phys. Rev. C **71**, 044906 (2005), arXiv:nucl-ex/0411036.
- [27] S. Afanasiev *et al.* (PHENIX), Source breakup dynamics in Au+Au Collisions at $s(\text{NN})^{1/2} = 200$ -GeV via three-dimensional two-pion source imaging, Phys. Rev. Lett. **100**, 232301 (2008), arXiv:0712.4372 [nucl-ex].
- [28] G. Verde, D. A. Brown, P. Danielewicz, C. K. Gelbke, W. G. Lynch, and M. B. Tsang, Imaging sources with fast and slow emission components, Phys. Rev. C **65**, 054609 (2002), arXiv:nucl-ex/0112004.
- [29] D. A. Brown and P. Danielewicz, Observing nongaussian sources in heavy ion reactions, Phys. Rev. C **64**, 014902 (2001), arXiv:nucl-th/0010108.
- [30] P. Nizabimana and P. Danielewicz, Source function from two-particle correlation through deblurring, Phys. Lett. B **846**, 138247 (2023), arXiv:2307.00173 [nucl-th].
- [31] N. J. Abdulameer *et al.* (PHENIX), Centrality dependence of Lévy-stable two-pion Bose-Einstein correlations in $s_{\text{NN}}=200$ GeV Au+Au collisions, Phys. Rev. C **110**, 064909 (2024), arXiv:2407.08586 [nucl-ex].
- [32] D. Kincses (STAR), Pion Interferometry with Lévy-Stable Sources in $= 200$ GeV Au + Au Collisions at STAR, Universe **10**, 102 (2024), arXiv:2401.11169 [nucl-ex].
- [33] A. Adare *et al.* (PHENIX), Lévy-stable two-pion Bose-Einstein correlations in $\sqrt{s_{\text{NN}}} = 200$ GeV Au+Au collisions, Phys. Rev. C **97**, 064911 (2018), [Erratum: Phys. Rev. C **108**, 049905 (2023)], arXiv:1709.05649 [nucl-ex].
- [34] A. Tumasyan *et al.* (CMS), Two-particle Bose-Einstein correlations and their Lévy parameters in PbPb collisions at $s_{\text{NN}}=5.02$ TeV, Phys. Rev. C **109**, 024914 (2024), arXiv:2306.11574 [nucl-ex].
- [35] H. Adhikary *et al.* (NA61/SHINE), Two-pion femto-

- scopic correlations in Be+Be collisions at $\sqrt{s_{NN}} = 16.84$ GeV measured by the NA61/SHINE at CERN, Eur. Phys. J. C **83**, 919 (2023), arXiv:2302.04593 [nucl-ex].
- [36] D. Kincses, M. Nagy, and M. Csanád, Lévy walk of pions in heavy-ion collisions, Commun. Phys. **8**, 55 (2025), arXiv:2409.10373 [nucl-th].
- [37] M. Csanád and D. Kincses, Investigating the excitation function of HBT radii for Lévy-stable sources, J. Phys. G **52**, 025102 (2025), arXiv:2406.11435 [nucl-th].
- [38] B. Kórodi, D. Kincses, and M. Csanád, Event-by-event investigation of the two-particle source function in sNN=2.76 TeV PbPb collisions with EPOS, Phys. Lett. B **847**, 138295 (2023), arXiv:2212.02980 [nucl-th].
- [39] D. Kincses, M. I. Nagy, and M. Csanád, Coulomb and strong interactions in the final state of Hanbury-Brown–Twiss correlations for Lévy-type source functions, Phys. Rev. C **102**, 064912 (2020), arXiv:1912.01381 [hep-ph].
- [40] R. Hanbury Brown and R. Q. Twiss, A New type of interferometer for use in radio astronomy, Phil. Mag. Ser. 7 **45**, 663 (1954).
- [41] R. Hanbury Brown and R. Q. Twiss, A Test of a new type of stellar interferometer on Sirius, Nature **178**, 1046 (1956).
- [42] B. Kurgyis (PHENIX), Three dimensional Lévy HBT results from PHENIX, *13th Workshop on Particle Correlations and Femtoscopy*, Acta Physica Polonica B Proceedings Supplement **12**, 10.5506/APhysPolBSupp.12.477 (2019), arXiv:1809.09392 [nucl-ex].
- [43] E. Mount, G. Graef, M. Mitrovski, M. Bleicher, and M. A. Lisa, Correspondence between hanbury-brown–twiss radii and the emission zone in noncentral heavy ion collisions, Phys. Rev. C **84**, 014908 (2011).
- [44] M. Csanád, B. Tomášik, and T. Csörgő, Interplay among the azimuthally dependent HBT radii and the elliptic flow, Eur. Phys. J. A **37**, 111 (2008), arXiv:0801.4434 [nucl-th].
- [45] J. Cimerman, B. Tomášik, M. Csanád, and S. Lökös, Higher-order anisotropies in the Blast-Wave Model - disentangling flow and density field anisotropies, Eur. Phys. J. A **53**, 161 (2017), arXiv:1702.01735 [nucl-th].
- [46] S. Lökös, M. Csanád, B. Tomášik, and T. Csörgő, Higher order anisotropies in the Buda-Lund model: Disentangling flow and density field anisotropies, Eur. Phys. J. A **52**, 311 (2016), arXiv:1604.07470 [nucl-th].
- [47] L. Adamczyk *et al.* (STAR), Beam-energy-dependent two-pion interferometry and the freeze-out eccentricity of pions measured in heavy ion collisions at the STAR detector, Phys. Rev. C **92**, 014904 (2015), arXiv:1403.4972 [nucl-ex].
- [48] D. Adamova *et al.* (ALICE), Azimuthally differential pion femtoscopy in Pb-Pb collisions at $\sqrt{s_{NN}} = 2.76$ TeV, Phys. Rev. Lett. **118**, 222301 (2017), arXiv:1702.01612 [nucl-ex].
- [49] U. Heinz, A. Hummel, M. A. Lisa, and U. A. Wiedemann, Symmetry constraints for the emission angle dependence of hanbury–brown–twiss radii, Phys. Rev. C **66**, 044903 (2002).
- [50] Y. Khyzhniak and M. A. Lisa, Pair momentum dependence of a tilted source in heavy-ion collisions, Phys. Rev. C **111**, 024902 (2025), arXiv:2410.15134 [nucl-th].
- [51] F. Retiere and M. A. Lisa, Observable implications of geometrical and dynamical aspects of freeze out in heavy ion collisions, Phys. Rev. C **70**, 044907 (2004), arXiv:nucl-th/0312024.
- [52] C. Lucarelli (LHCb), SMOG: a high-density gas target experiment at LHCb, PoS **ICHEP2024**, 588 (2025).
- [53] P. Di Nezza, V. Carassiti, G. Ciullo, R. Engels, P. Lenisa, L. L. Pappalardo, M. Santimaria, E. Steffens, and G. Tagliente, Fixed Target Program at the LHC, PoS **SPIN2023**, 036 (2024).
- [54] C. Hadjidakis *et al.*, High-luminosity fixed-target experiments at the LHC, PoS **HardProbes2018**, 041 (2019), arXiv:1902.10534 [hep-ex].
- [55] Z.-W. Lin, C. M. Ko, B.-A. Li, B. Zhang, and S. Pal, Multiphase transport model for relativistic heavy ion collisions, Phys. Rev. C **72**, 064901 (2005).
- [56] D. d’Enterria and C. Loizides, Progress in the Glauber Model at Collider Energies, Ann. Rev. Nucl. Part. Sci. **71**, 315 (2021), arXiv:2011.14909 [hep-ph].
- [57] G. Giacalone, B. Bally, G. Nijs, S. Shen, T. Duguet, J.-P. Ebran, S. Elhatisari, M. Frosini, T. A. Lähde, D. Lee, B.-N. Lu, Y.-Z. Ma, U.-G. Meißner, J. Noronha-Hostler, C. Plumberg, T. R. Rodríguez, R. Roth, W. van der Schee, and V. Somà, *The unexpected uses of a bowling pin: exploiting ^{20}Ne isotopes for precision characterizations of collectivity in small systems*, Tech. Rep. (2024) arXiv:2402.05995.
- [58] Z. Lu, M. Zhao, E. G. D. Nielsen, X. Li, and Y. Zhou, Signature of the α -clustering structure of light nuclei in relativistic nuclear collisions (2025), arXiv:2501.14852 [nucl-th].
- [59] G. Giacalone *et al.*, Anisotropic Flow in Fixed-Target Pb208+Ne20 Collisions as a Probe of Quark-Gluon Plasma, Phys. Rev. Lett. **134**, 082301 (2025), arXiv:2405.20210 [nucl-th].
- [60] E. Árpási and M. I. Nagy, Multi-dimensional investigation of the pion pair-source in heavy-ion collisions with epos, International Journal of Modern Physics A **0**, 2542001 (0), <https://doi.org/10.1142/S0217751X25420011>.
- [61] J. He, S. Zhang, Y.-G. Ma, J. Chen, and C. Zhong, Clustering structure effect on Hanbury-Brown–Twiss correlation in $^{12}\text{C}+^{197}\text{Au}$ collisions at 200 GeV, Eur. Phys. J. A **56**, 52 (2020), arXiv:2002.06058 [nucl-th].